NASA TECHNICAL MEMORANDUM

NASA TM X-2770

NASA TM X-2770

NONLINEAR EQUATIONS FOR BENDING OF ROTATING BEAMS WITH APPLICATION TO LINEAR FLAP-LAG STABILITY OF HINGELESS ROTORS

by Dewey H. Hodges and Robert A. Ormiston

Ames Research Center

and

U.S. Army Air Mobility R&D Laboratory

Moffett Field, Calif. 94035

NATIONAL AERONAUTICS AND SPACE ADMINISTRATION • WASHINGTON, D. C. • MAY 1973

1. Report No.	2. Government Accession No.	3. Recipient's Catalog No.
NASA TM X–2770		

4. Title and Subtitle	5. Report Date
NONLINEAR EQUATIONS FOR BENDING OF ROTATING BEAMS WITH APPLICATION TO LINEAR FLAP–LAG STABILITY OF HINGELESS ROTORS	May 1973
	6. Performing Organization Code

7. Author(s)	8. Performing Organization Report No.
Dewey H. Hodges and Robert A. Ormiston	A–4629
	10. Work Unit No. 760–76–03–07–00

9. Performing Organization Name and Address	11. Contract or Grant No.
NASA Ames Research Center and U.S. Army Air Mobility R&D Laboratory Moffett Field, Calif., 94035	

12. Sponsoring Agency Name and Address	13. Type of Report and Period Covered
National Aeronautics and Space Administration Washington, D. C., 20546	Technical Memorandum
	14. Sponsoring Agency Code

15. Supplementary Notes

16. Abstract

The nonlinear partial differential equations for the flapping and lead-lag degrees of freedom of a torsionally rigid, rotating cantilevered beam are derived. These equations are linearized about an equilibrium condition to study the flap-lag stability characteristics of hingeless helicopter rotor blades with zero twist and uniform mass and stiffness in the hovering flight condition. The results indicate that these configurations are stable because the effect of elastic coupling more than compensates for the destabilizing flap-lag Coriolis and aerodynamic coupling. The effect of higher bending modes on the lead-lag damping was found to be small and the common, centrally hinged, spring restrained, rigid blade approximation for elastic rotor blades was shown to be reasonably satisfactory for determining flap-lag stability. The effect of pre-cone was generally stabilizing and the effects of rotary inertia were negligible.

17. Key Words (Suggested by Author(s))	18. Distribution Statement
Flap-lag stability Hingeless rotors Helicoptor rotors Rotating beams	Unclassified – Unlimited

19. Security Classif. (of this report)	20. Security Classif. (of this page)	21. No. of Pages	22. Price*
Unclassified	Unclassified	36	$3.00

* For sale by the National Technical Information Service, Springfield, Virginia 22151

SYMBOLS

a	lift-curve slope
A	cross-section area of blade, m^2
$A_i - F_{ijk}$	Galerkin integrals, equation (55)
b	number of blades
c	blade chord, m
c_{d_O}	drag coefficient
D	drag per unit length, N/m
e	longitudinal strain
E	Young's modulus, N/m^2
I	blade inertia integral, $\int_0^R mx^2 \, dx$, $kg \cdot m^2$
I_1	area moment of inertia, $\iint z'^2 \, dA$, m^4
I_2	area moment of inertia, $\iint y'^2 \, dA$, m^4
K	longitudinal stiffness parameter, $\frac{EA}{m\Omega^2 R^2}$
L	lift per unit length, N/m
L_x, L_y, L_z	components of generalized nonconservative forces per unit length, N/m
m	blade mass per unit length, kg/m
$\vec{n}_1, \vec{n}_2, \vec{n}_3$	unit vectors in x, y, z coordinate system
N	number of assumed bending modes
$\vec{Q}$	nonconservative force vector, N
$\vec{r}$	position vector of point on blade

R	length of blade, m
S_{ij}, T_{ij}	terms involving Galerkin integrals, equation (56)
t	time, sec
T	kinetic energy, $kg \cdot m^2/sec^2$
u, v, w	radial, lead-lag, and flap displacements of elastic axis, figure 1
U_P	fluid velocity component relative to blade cross section and perpendicular to plane of rotation, figure 3, m/sec
U_T	fluid velocity component relative to blade cross section and parallel to plane of rotation, figure 3, m/sec
$\vec{v}$	inertial velocity of a point on blade
v_i	induced velocity, m/sec
V	$\sqrt{U_P^2 + U_T^2}$, m/sec
x, y, z	rotor blade coordinate system, x coincident with elastic axis of undeformed blade, figure 1
X, Y, Z	rotating coordinate system, figure 1
y', z'	blade cross section principal axes, figure 2
β_j	generalized flapping coordinate, equation (51)
β_{pc}	pre-cone angle, rad, figure 1
γ	lock number, $\frac{\rho_\infty acR^4}{I}$
δW	virtual work of nonconservative forces
ϵ	longitudinal strain at the elastic axis, equation (21d)
ζ_j	generalized lead-lag coordinate, equation (51)
θ	blade pitch angle, rad
Λ_1	dimensionless flapwise bending stiffness parameter, $\sqrt{\frac{EI_1}{m\Omega^2 R^4}}$

Λ_2	dimensionless chordwise bending stiffness parameter, $\sqrt{\frac{EI_2}{m\Omega^2 R^4}}$
ξ	dimensionless radial coordinate, $\frac{x}{R}$
ρ	blade density, kg/m^3
ρ_∞	air density, kg/m^3
σ	solidity, $\frac{bc}{\pi R}$
τ	dimensionless time, Ωt
φ	aerodynamic inflow angle, figure 3
ω_j, f_j	mode shape parameters, table 1
$\omega_{\beta_{NR}}$	first nonrotating flap frequency, $\omega_1{}^2 \Lambda_1$, rad/sec
$\omega_{\zeta_{NR}}$	first nonrotating lead-lag frequency, $\omega_1{}^2 \Lambda_2$, rad/sec
ω_β, ω_ζ	imaginary part of eigenvalue for first flap and lead-lag bending modes, rad/sec
Ω	rotor blade angular velocity, rad/sec
σ_β, σ_ζ	real part of eigenvalue for first flap and lead-lag bending modes
$(\ )_o$	equilibrium quantity
$\Delta(\ )$	perturbation quantity
$(\ )'$	$\frac{d(\ )}{d\xi}$
$(\dot{\ })$	$\frac{d(\ )}{d\tau}$
$(\bar{\ })$	quantity made dimensionless by $m\Omega^2 R$ for force per unit length, R for length, ΩR for velocity, and Ω for frequencies and eigenvalues

NONLINEAR EQUATIONS FOR BENDING OF ROTATING BEAMS WITH APPLICATION TO LINEAR FLAP–LAG STABILITY OF HINGELESS ROTORS

Dewey H. Hodges and Robert A. Ormiston

Ames Research Center
and
U. S. Army Air Mobility R & D Laboratory
Moffett Field, California 94035

SUMMARY

The nonlinear partial differential equations for the flapping and lead-lag degrees of freedom of a torsionally rigid, rotating cantilevered beam are derived. These equations are linearized about an equilibrium condition to study the flap-lag stability characteristics of hingeless helicopter rotor blades with zero twist and uniform mass and stiffness in the hovering flight condition. The results indicate that these configurations are stable because the effect of elastic coupling more than compensates for the destabilizing flap-lag Coriolis and aerodynamic coupling. The effect of higher bending modes on the lead-lag damping was found to be small and the common, centrally hinged, spring restrained, rigid blade approximation for elastic rotor blades was shown to be reasonably satisfactory for determining flap-lag stability. The effect of pre-cone was generally stabilizing and the effects of rotary inertia were negligible.

INTRODUCTION

Helicopter rotor blades that are cantilevered to the rotor hub can substantially improve helicopter flying qualities by increasing rotor control power and angular damping. This type of rotor is known as a hingeless rotor because it lacks the flapping and lead-lag hinges found on conventional articulated rotors. The absence of such hinges requires the blades to bend elastically in two directions: perpendicular (flapping) and parallel (lead-lag) to the plane of the rotor for centrifugal relief of aerodynamic forces. In general, the bending deflections are also accompanied by torsional deformations of the blade.

Although experience with hingeless rotors is not extensive, previous research has indicated that for certain configurations, the coupling between the flapping and lead-lag degrees of freedom may result in unstable oscillations (refs. 1 and 2). This condition is known as flap-lag instability. It is a restricted case of the general hingeless rotor blade stability problem because the torsion degree of freedom is not included. This restricted problem is quite useful, however, because it gives considerable insight into the coupling mechanisms of flap-lag motion which can contribute to rotor blade instabilities. These coupling mechanisms are primarily due to the combination of aerodynamic

and inertial coupling (Coriolis and centrifugal), which is essentially proportional to the mean flapping or coning of the rotor blade. Since the coning increases with rotor thrust, flap-lag stability is of most interest for moderate to high thrust conditions. The Coriolis and centrifugal inertial forces are basically nonlinear but can be linearized for small oscillations about the mean flapping and lead-lag deflections.

The prominent feature of previous research (refs. 1 and 2) is a method of approximating the continuous elastic bending deflections of a hingeless rotor blade with a centrally hinged, spring restrained, rigid blade. Such an approximation reduces the problem from one of partial differential equations to one involving only ordinary differential equations. The solutions then become simpler to obtain and the results are somewhat easier to interpret in physical terms. Another important reason for using the approximate rigid blade representation is that equations suitable for the elastic bending of rotating beams including the nonlinear effects noted above have not been available, whereas the nonlinear rigid blade equations are relatively easy to derive. The most general linear treatment for the elastic rotating beam may be found in reference 3.

The purpose of the present report, therefore, is to derive a suitable system of nonlinear equations for the flapping and lead-lag bending degrees of freedom of a torsionally rigid, rotating cantilever beam. A general treatment of the nonlinear inertial forces requires an additional degree of freedom for radial deflections of the blade and use of a nonlinear radial strain equation valid for large bending deflections. The radial degree of freedom is ultimately expressed in terms of the two bending deflections so that the final equations contain only the two primary degrees of freedom. A procedure for linearizing the equations about a particular equilibrium condition is given and results for the stability of various untwisted rotor blade configurations with uniform mass and stiffness are presented in the hovering flight condition. In addition to revealing the stability characteristics of elastic hingeless rotor blades, these results will also serve to establish the accuracy of the common rigid blade representation of a hingeless rotor blade.

One result of reference 2 indicated that flap-lag instabilities were highly sensitive to the elastic coupling between the flap and lead-lag degrees of freedom. For the rigid blade representation, this coupling could be controlled by varying the orientation of the flap and lead-lag restraint springs at the blade hinges. For the actual elastic blade, the analogous elastic coupling effect is dependent on the orientation of the elastic principal axes of the rotor blade cross section and the radial distribution of bending stiffness. The results of reference 2 showed that when the restraint springs of the rigid blade model were configured to represent untwisted, uniform stiffness cantilever blades, the flap-lag instability was suppressed. Since the present numerical results are restricted to uniform untwisted blades, it is expected that unstable oscillations will not be encountered. However, in addition to flap-lag stability, the damping of the lead-lag bending motion is of considerable practical importance because the inherent aerodynamic and structural lead-lag damping of hingeless rotors is very small. This leads to potentially high fatigue stresses and vibration, and increases the susceptibility of the helicopter to coupled rotor-airframe instabilities. The results to be presented will compare lead-lag damping of the rigid blade representation with the elastic blade and examine the sensitivity of the elastic blade damping to the number of bending modes included.

EQUATIONS OF MOTION

The equations of motion for a rotating cantilevered beam, rigid in torsion, are derived using Hamilton's variational principle. They include three nonlinear equations for radial, lead-lag, and flapping displacements, u, v, and w, respectively. Aerodynamic forces are represented as a distributed generalized loading and are derived from simple quasi-steady strip theory. The initial derivation is valid for beams with variable mass and stiffness properties, pre-cone, and twist; however, for the present purposes it is sufficient to consider only untwisted configurations with uniform mass and stiffness. The resulting nonlinear equations can be linearized for small perturbations about a steady-state operating condition. This enables the radial displacement u to be eliminated from the equations of motion leaving only the primary flap and lead-lag displacements. The final perturbation equations are linear variable coefficient integro-partial differential equations, which are solved by Galerkin's method.

Variational Formulation

Coordinate systems– The X, Y, Z coordinate system, figure 1, rotates with constant angular velocity about the Z axis and its origin is fixed in inertial space. The plane of rotation is defined by the X, Y axes. The position of a beam S is defined in a second x, y, z coordinate system, with the x axis coincident with the undeformed position of the beam and rotated about the Y axis through an angle β_{pc}, the pre-cone angle.

The displacements of the beam elastic axis u, v, w are defined along the unit vectors $\vec{n}_1$, $\vec{n}_2$, $\vec{n}_3$, which are parallel to x, y, z, respectively. The beam is cantilevered at the origin and the elastic axis, aerodynamic centers, and mass centers are coincident with the x axis in the undeformed state. The beam pitch angle θ, which defines the orientation of the cross section principal axes y' and z', is shown in figure 2. For an arbitrary displacement, the position vector of a point on the beam will be

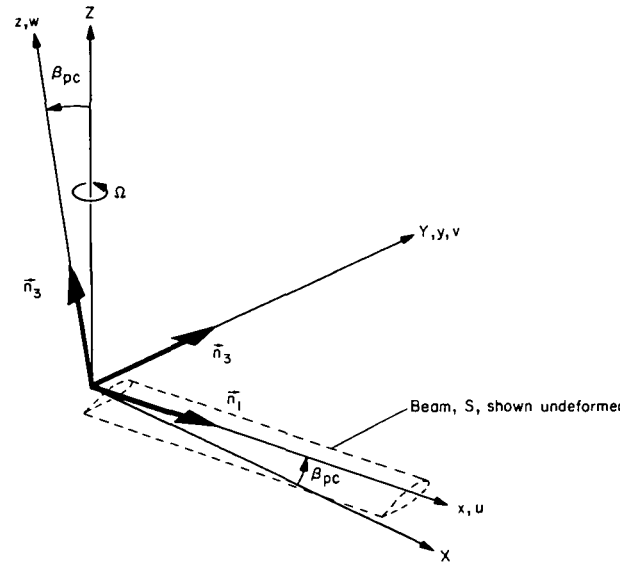

Figure 1.– Coordinate systems.

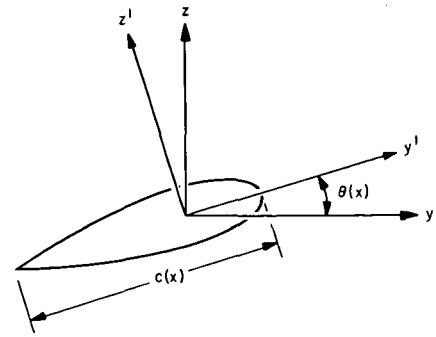

Figure 2.– Blade cross-section coordinate system.

$$\vec{r} = \left(x + u - y\,\frac{\partial v}{\partial x} - z\,\frac{\partial w}{\partial x}\right)\vec{n}_1$$

$$+ (v + y)\vec{n}_2 + (w + z)\vec{n}_3 \qquad (1)$$

This equation assumes that squares of bending slopes are negligible with respect to unity and that plane sections remain plane. The radial elongation of the beam $\partial u/\partial x$ is assumed to be of order $(\partial v/\partial x)^2$ and $(\partial w/\partial x)^2$ and thus can also be neglected with respect to unity. Similar reasoning applies to terms of order $(y/R)^2$ and $(z/R)^2$.

Kinetic energy— The velocity of a point on the blade with respect to inertial space is

$$\vec{v} = \frac{\delta \vec{r}}{\delta t} + \vec{\Omega} \times \vec{r} \tag{2}$$

The first term is the velocity with respect to the rotating x, y, z coordinate system.

$$\frac{\delta \vec{r}}{\delta t} = \left(\frac{\partial u}{\partial t} - y\,\frac{\partial^2 v}{\partial x\,\partial t} - z\,\frac{\partial^2 w}{\partial x\,\partial t}\right)\vec{n}_1 + \frac{\partial v}{\partial t}\,\vec{n}_2 + \frac{\partial w}{\partial t}\,\vec{n}_3 \tag{3}$$

The second term due to the coordinate system rotation is

$$\vec{\Omega} \times \vec{r} = -\Omega \cos \beta_{pc}(v + y)\vec{n}_1 + \left[\Omega \cos \beta_{pc}\left(x + u - y\,\frac{\partial v}{\partial x} - z\,\frac{\partial w}{\partial x}\right)\right.$$

$$\left. - \Omega \sin \beta_{pc}(w + z)\right]\vec{n}_2 + \Omega \sin \beta_{pc}(v + y)\vec{n}_3 \tag{4}$$

The velocity is therefore

$$\vec{v} = \left[\frac{\partial u}{\partial t} - \Omega \cos \beta_{pc}(v + y) - y\,\frac{\partial^2 v}{\partial x\,\partial t} - z\,\frac{\partial^2 w}{\partial x\,\partial t}\right]\vec{n}_1$$

$$+ \left[\frac{\partial v}{\partial t} + \Omega \cos \beta_{pc}\left(x + u - y\,\frac{\partial v}{\partial x} - z\,\frac{\partial w}{\partial x}\right) - \Omega \sin \beta_{pc}(w + z)\right]\vec{n}_2$$

$$+ \left[\frac{\partial w}{\partial t} + \Omega \sin \beta_{pc}(v + y)\right]\vec{n}_3 \tag{5}$$

The kinetic energy is

$$T \equiv \frac{1}{2}\int\int\int_S \rho \vec{v} \cdot \vec{v}\, dx\, dy\, dz \tag{6}$$

and its first variation is

$$\delta T \equiv \iiint \rho \vec{v} \cdot \delta \vec{v} \, dx \, dy \, dz \tag{7}$$

where

$$\delta \vec{v} = \left(\frac{\partial \delta u}{\partial t} - \Omega \cos \beta_{pc} \delta v - y \frac{\partial^2 \delta v}{\partial x \, \partial t} - z \frac{\partial^2 \delta w}{\partial x \, \partial t} \right) \vec{n}_1$$

$$+ \left[\frac{\partial \delta v}{\partial t} + \Omega \cos \beta_{pc} \left(\delta u - y \frac{\partial \delta v}{\partial x} - z \frac{\partial \delta w}{\partial x} \right) - \Omega \sin \beta_{pc} \delta w \right] \vec{n}_2$$

$$+ \left(\frac{\partial \delta w}{\partial t} + \Omega \sin \beta_{pc} \delta v \right) \vec{n}_3 \tag{8}$$

From the cross section geometry of figure 2

$$\begin{aligned} y &= y' \cos \theta - z' \sin \theta \\ z &= y' \sin \theta + z' \cos \theta \end{aligned} \tag{9}$$

Substituting equations (5), (8), and (9) into (7) yields the following expression for δT. All quantities of order $(\partial v/\partial x)^2$ are ignored with respect to one.

$$\delta T = \int_0^R m \left\{ \left(\frac{\partial u}{\partial t} - \Omega v \cos \beta_{pc} \right) \frac{\partial \delta u}{\partial t} + \left(\frac{\partial v}{\partial t} + \Omega x \cos \beta_{pc} + \Omega u \cos \beta_{pc} - \Omega w \sin \beta_{pc} \right) \frac{\partial \delta v}{\partial t} \right.$$

$$+ \left(\frac{\partial w}{\partial t} + \Omega v \sin \beta_{pc} \right) \frac{\partial \delta w}{\partial t} + \left[\frac{\partial v}{\partial t} + \Omega (x + u) \cos \beta_{pc} - \Omega w \sin \beta_{pc} \right] \Omega \cos \beta_{pc} \delta u$$

$$+ \left[\left(\frac{\partial w}{\partial t} + \Omega v \sin \beta_{pc} \right) \Omega \sin \beta_{pc} - \left(\frac{\partial u}{\partial t} - \Omega v \cos \beta_{pc} \right) \Omega \cos \beta_{pc} \right] \delta v$$

$$\left. - \left[\frac{\partial v}{\partial t} + \Omega (x + u) \cos \beta_{pc} - \Omega w \sin \beta_{pc} \right] \Omega \sin \beta_{pc} \delta w \right\} dx \tag{10}$$

where

$$m \equiv \iint \rho \, dy' \, dz' \tag{11}$$

Note that due to symmetry properties of the cross section, the following integrals are equal to zero

$$\iint y'\,dy'\,dz',\ \iint z'\,dy'\,dz',\ \iint y'z'\,dy'\,dz'$$

Because higher order terms were discarded, the kinetic energy expression does not include contributions of rotary inertia. Although this is a very small effect for rotor blade configurations, the rotary inertia terms were included for calculation of certain results to be discussed below.

Strain energy– Previous derivations of rotor blade equations restricted to the case of small deflections have employed linear strain–displacement relations. Because the present derivation is addressed to the flap-lag stability problem with moderately large displacements, the linear relations are not valid. The following strain–displacement relation is used, which has been modified from reference 3 by the inclusion of the underlined nonlinear terms:

$$e \equiv \frac{\partial u}{\partial x} + \underline{\frac{1}{2}\left(\frac{\partial v}{\partial x}\right)^2 + \frac{1}{2}\left(\frac{\partial w}{\partial x}\right)^2} - y'\left(\frac{\partial^2 v}{\partial x^2}\cos\theta + \frac{\partial^2 w}{\partial x^2}\sin\theta\right) + z'\left(\frac{\partial^2 v}{\partial x^2}\sin\theta - \frac{\partial^2 w}{\partial x^2}\cos\theta\right) \tag{12}$$

For long, slender beams, the strain energy is independent of the shear modulus and is simply

$$U \equiv \iiint_S \frac{Ee^2}{2}\,dx\,dy\,dz \tag{13}$$

The first variation is

$$\delta U = \iiint_S Ee\delta e\,dx\,dy\,dz \tag{14}$$

where

$$\delta e = \frac{\partial \delta u}{\partial x} + \frac{\partial v}{\partial x}\frac{\partial \delta v}{\partial x} + \frac{\partial w}{\partial x}\frac{\partial \delta w}{\partial x} - y'\left(\frac{\partial^2 \delta v}{\partial x^2}\cos\theta + \frac{\partial^2 \delta w}{\partial x^2}\sin\theta\right) + z'\left(\frac{\partial^2 \delta v}{\partial x^2}\sin\theta - \frac{\partial^2 \delta w}{\partial x^2}\cos\theta\right) \tag{15}$$

Substituting equations (12) and (15) into (14) and using equation (9), we obtain:

$$\delta U = \int_0^R \left\{ EA\left[\frac{\partial u}{\partial x} + \frac{1}{2}\left(\frac{\partial v}{\partial x}\right)^2 + \frac{1}{2}\left(\frac{\partial w}{\partial x}\right)^2\right]\left(\frac{\partial \delta u}{\partial x} + \frac{\partial v}{\partial x}\frac{\partial \delta v}{\partial x} + \frac{\partial w}{\partial x}\frac{\partial \delta w}{\partial x}\right)\right.$$

$$+ EI_2\left(\frac{\partial^2 v}{\partial x^2}\cos\theta + \frac{\partial^2 w}{\partial x^2}\sin\theta\right)\left(\frac{\partial^2 \delta v}{\partial x^2}\cos\theta + \frac{\partial^2 \delta w}{\partial x^2}\sin\theta\right)$$

$$\left. + EI_1\left(\frac{\partial^2 v}{\partial x^2}\sin\theta - \frac{\partial^2 w}{\partial x^2}\cos\theta\right)\left(\frac{\partial^2 \delta v}{\partial x^2}\sin\theta - \frac{\partial^2 \delta w}{\partial x^2}\cos\theta\right)\right\} dx \tag{16}$$

Nonconservative forces– The virtual work δW of the nonconservative forces is usually expressed as a time integral:

$$\int_{t_1}^{t_2} \delta W \, dt = \int_{t_1}^{t_2} \vec{Q} \cdot \delta\vec{q} \, dt \tag{17}$$

where $\vec{Q}$ is the vector of applied distributed loads and $\delta\vec{q}$ is the vector of virtual displacements. Hence,

$$\int_{t_1}^{t_2} \delta W \, dt = \int_{t_1}^{t_2} \int_0^R (L_X \delta u + L_y \delta v + L_Z \delta w) dx \, dt \tag{18}$$

where L_X, L_y, L_Z, and δu, δv, δw are the components of $\vec{Q}$ and $\delta\vec{q}$, respectively.

General equations– Hamilton's variational principle is stated as follows:

$$\int_{t_1}^{t_2} [\delta T - \delta U + \delta W] \, dt = 0 \tag{19}$$

We now substitute equations (10), (16), and (18) into equation (19) and perform, by parts, all integrations that are necessary to obtain an expression of the form

$$\int_{t_1}^{t_2} \int_0^R [(\quad)\delta u + (\quad)\delta v + (\quad)\delta w] \, dx \, dt + \text{boundary terms} = 0 \tag{20}$$

For arbitrary, admissible variations δu, δv, δw, the three expressions in parentheses must vanish individually (as well as the boundary conditions). This entire series of operations yields the following three nonlinear partial differential equations:

$$-\frac{\partial}{\partial x}(EA\epsilon) - m\left(2\Omega\frac{\partial v}{\partial t} + \Omega^2 x\right) = L_x \tag{21a}$$

$$-\frac{\partial}{\partial x}\left(EA\epsilon\,\frac{\partial v}{\partial x}\right) + \frac{\partial}{\partial x^2}\left[(EI_2\cos^2\theta + EI_1\sin^2\theta)\frac{\partial^2 v}{\partial x^2} + (EI_2 - EI_1)\sin\theta\cos\theta\frac{\partial^2 w}{\partial x^2}\right]$$

$$+ m\left[\frac{\partial^2 v}{\partial t^2} - \Omega^2 v + 2\Omega\left(\frac{\partial u}{\partial t} - \beta_{pc}\frac{\partial w}{\partial t}\right)\right] = L_y \tag{21b}$$

$$-\frac{\partial}{\partial x}\left(EA\epsilon\,\frac{\partial w}{\partial x}\right) + \frac{\partial}{\partial x^2}\left[(EI_2 - EI_1)\cos\theta\sin\theta\frac{\partial^2 v}{\partial x^2} + (EI_2\sin^2\theta + EI_1\cos^2\theta)\frac{\partial^2 w}{\partial x^2}\right]$$

$$+ m\left(\frac{\partial^2 w}{\partial t^2} + \Omega^2\beta_{pc}x + 2\Omega\beta_{pc}\frac{\partial v}{\partial t}\right) = L_z \tag{21c}$$

where

$$\epsilon = \frac{\partial u}{\partial x} + \frac{1}{2}\left(\frac{\partial v}{\partial x}\right)^2 + \frac{1}{2}\left(\frac{\partial w}{\partial x}\right)^2 \tag{21d}$$

Note that ϵ is the strain at the elastic axis. In obtaining the equations, the small angle assumption has been invoked for the pre-cone angle, $\sin\beta_{pc} \cong \beta_{pc}$, $\beta_{pc}^2 << 1$. These equations are nonlinear, partial differential equations of fourth order with variable coefficients in x, and of second order in t.

Linearization of the Equations

Before the equations are linearized, they are restricted to configurations with untwisted blades and uniform mass and stiffness properties. The equations will also be made dimensionless by dividing through by $m\Omega^2 R$. The dimensionless displacements, u, v, w are then based on the rotor blade radius R, and the independent variables become $\xi = x/R$ and $\tau = \Omega t$. The radial aerodynamic force component L_X is of second order for small θ and w', and consistent with second-order structural terms, can be discarded. The equations are:

$$-K\frac{\partial\epsilon}{\partial\xi}-\xi-2\frac{\partial\bar{v}}{\partial\tau}=0 \tag{22a}$$

$$-K\frac{\partial}{\partial\xi}\left(\epsilon\frac{\partial\bar{v}}{\partial\xi}\right)+\bar{\Lambda}_2{}^2\frac{\partial^4\bar{v}}{\partial\xi^4}+\bar{\Lambda}_{12}\frac{\partial^4\bar{w}}{\partial\xi^4}+\frac{\partial^2\bar{v}}{\partial\tau^2}-\bar{v}+2\left(\frac{\partial\bar{u}}{\partial\tau}-\beta_{pc}\frac{\partial\bar{w}}{\partial\tau}\right)=\bar{L}_y \tag{22b}$$

$$-K\frac{\partial}{\partial\xi}\left(\epsilon\frac{\partial\bar{w}}{\partial\xi}\right)+\bar{\Lambda}_{12}\frac{\partial^4\bar{v}}{\partial\xi^4}+\bar{\Lambda}_1{}^2\frac{\partial^4\bar{w}}{\partial\xi^4}+\frac{\partial^2\bar{w}}{\partial\tau^2}+\beta_{pc}\left(\xi+2\frac{\partial\bar{v}}{\partial\tau}\right)=\bar{L}_z \tag{22c}$$

where

$$\epsilon=\frac{\partial\bar{u}}{\partial\xi}+\frac{1}{2}\left(\frac{\partial\bar{v}}{\partial\xi}\right)^2+\frac{1}{2}\left(\frac{\partial\bar{w}}{\partial\xi}\right)^2 \tag{22d}$$

and

$$\left.\begin{aligned}
\bar{\Lambda}_1{}^2&\equiv\Lambda_1{}^2\cos^2\theta+\Lambda_2{}^2\sin^2\theta\\
\bar{\Lambda}_2{}^2&\equiv\Lambda_1{}^2\sin^2\theta+\Lambda_2{}^2\cos^2\theta\\
\bar{\Lambda}_{12}&\equiv(\Lambda_2{}^2-\Lambda_1{}^2)\cos\theta\sin\theta\\
\Lambda_1{}^2&\equiv EI_1/m\Omega^2R^4\\
\Lambda_2{}^2&\equiv EI_2/m\Omega^2R^4\\
K&\equiv EA/m\Omega^2R^2\\
\bar{L}_y&\equiv L_y/m\Omega^2R\\
\bar{L}_z&\equiv L_z/m\Omega^2R
\end{aligned}\right\} \tag{22e}$$

The terms defined in equation (22e) are the dimensionless aerodynamic forces and elastic section properties. Note that θ is now the blade pitch angle, and is constant over the radius. The parameter K is the ratio of longitudinal elastic forces to centrifugal forces, whereas $\Lambda_1{}^2$ and $\Lambda_2{}^2$ are the ratios of the section bending stiffness to the centrifugal forces. Examination of the equations reveals that tensile forces are associated with K, while $\Lambda_1{}^2$, $\Lambda_2{}^2$ identify the elastic bending terms. These equations differ from previous results (ref. 3) in two ways. First, the radial force equation includes the centrifugal term due to lead-lag velocity ($-2(\partial\bar{v}/\partial\tau)$). This means that the tension (or strain ϵ) terms in the flap and lead-lag equations are nonlinear, because ϵ is a function of lead-lag displacement. Second, the retention of the radial displacement u in the lead-lag equation produces the Coriolis forces that are responsible for the destabilizing effects on flap-lag oscillations. The radial displacement u is related to the longitudinal strain ϵ and the flap and lead-lag displacements by the nonlinear strain-displacement relation.

The nonlinear equations may be linearized about a suitable equilibrium operating condition without losing the essential features of the nonlinear flap-lag inertial coupling. The displacements are assumed to consist of the sum of time-independent parts and the time-dependent parts. These are, respectively, the steady-state equilibrium displacements and the perturbation displacements:

$$\left.\begin{aligned} \bar{u}(\xi, \tau) &= \bar{u}_0(\xi) + \Delta\bar{u}(\xi, \tau) \\ \bar{v}(\xi, \tau) &= \bar{v}_0(\xi) + \Delta\bar{v}(\xi, \tau) \\ \bar{w}(\xi, \tau) &= \bar{w}_0(\xi) + \Delta\bar{w}(\xi, \tau) \end{aligned}\right\} \tag{23}$$

Also, it is assumed that

$$\left.\begin{aligned} \epsilon(\xi, \tau) &= \epsilon_0(\xi) + \Delta\epsilon(\xi, \tau) \\ \bar{L}_y(\xi, \tau) &= \bar{L}_{y0}(\xi) + \Delta\bar{L}_y(\xi, \tau) \\ \bar{L}_z(\xi, \tau) &= \bar{L}_{z0}(\xi) + \Delta\bar{L}_z(\xi, \tau) \end{aligned}\right\} \tag{24}$$

The equations that result after substituting equations (23) and (24) into equations (22), and setting all perturbation quantities equal to zero, are called equilibrium equations. The equations that result from making the full substitution of equations (23) and (24), subtracting the equilibrium equations and discarding higher order products of perturbation quantities, are called the perturbation equations. The equilibrium equations are

$$-K\frac{d\epsilon_0}{d\xi} - \xi = 0 \tag{25a}$$

$$-K\frac{d}{d\xi}\left(\epsilon_0\frac{d\bar{v}_0}{d\xi}\right) + \bar{\Lambda}_2{}^2\frac{d^4\bar{v}_0}{d\xi^4} + \bar{\Lambda}_{12}\frac{d^4\bar{w}_0}{d\xi^4} - \bar{v}_0 = \bar{L}_{y0} \tag{25b}$$

$$-K\frac{d}{d\xi}\left(\epsilon_0\frac{d\bar{w}_0}{d\xi}\right) + \bar{\Lambda}_{12}\frac{d^4\bar{v}_0}{d\xi^4} + \bar{\Lambda}_1{}^2\frac{d^4\bar{w}_0}{d\xi^4} = \bar{L}_{z0} - \beta_{pc}\xi \tag{25c}$$

where

$$\epsilon_0 \equiv \frac{d\bar{u}_0}{d\xi} + \frac{1}{2}\left(\frac{d\bar{v}_0}{d\xi}\right)^2 + \frac{1}{2}\left(\frac{d\bar{w}_0}{d\xi}\right)^2 \tag{25d}$$

and the perturbation equations are

$$-K\frac{\partial \Delta\epsilon}{\partial \xi} - 2\frac{\partial \Delta\bar{v}}{\partial \tau} = 0 \tag{26a}$$

$$-K\frac{\partial}{\partial \xi}\left(\Delta\epsilon\,\frac{d\bar{v}_0}{d\xi}\right) - K\frac{\partial}{\partial \xi}\left(\epsilon_0\,\frac{\partial \Delta\bar{v}}{\partial \xi}\right) + \bar{\Lambda}_2{}^2\,\frac{\partial^4 \Delta\bar{v}}{\partial \xi^4} + \bar{\Lambda}_{12}\,\frac{\partial^4 \Delta\bar{w}}{\partial \xi^4} + \frac{\partial^2 \Delta\bar{v}}{\partial \tau^2} - \Delta\bar{v} + 2\frac{\partial \Delta\bar{u}}{\partial \tau}$$

$$- 2\beta_{pc}\frac{\partial \Delta\bar{w}}{\partial \tau} = \Delta\bar{L}_y \tag{26b}$$

$$-K\frac{\partial}{\partial \xi}\left(\Delta\epsilon\,\frac{d\bar{w}_0}{d\xi}\right) - K\frac{\partial}{\partial \xi}\left(\epsilon_0\,\frac{\partial \Delta\bar{w}}{\partial \xi}\right) + \bar{\Lambda}_{12}\,\frac{\partial^4 \Delta\bar{v}}{\partial \xi^4} + \bar{\Lambda}_1{}^2\,\frac{\partial^4 \Delta\bar{w}}{\partial \xi^4} + \frac{\partial^2 \Delta\bar{w}}{\partial \tau^2} + 2\beta_{pc}\frac{\partial \Delta\bar{v}}{\partial \tau} = \Delta\bar{L}_z \tag{26c}$$

where

$$\Delta\epsilon = \frac{\partial \Delta\bar{u}}{\partial \xi} + \frac{d\bar{v}_0}{d\xi}\,\frac{\partial \Delta\bar{v}}{\partial \xi} + \frac{d\bar{w}_0}{d\xi}\,\frac{\partial \Delta\bar{w}}{\partial \xi} \tag{26d}$$

Except for the equilibrium nonlinear strain equation (25d), the radial displacement u_0 does not appear in either set of equations. Therefore, a solution for u_0 is not required and equation (25d) is superfluous. The radial force equilibrium equation may be integrated and used to eliminate ϵ_0 in the remaining equations. Equation (25a) yields

$$\epsilon_0 = \frac{1 - \xi^2}{2K} \tag{27}$$

Substituting this equation into equations (25b) and (25c) yields the following equations for flap and lead-lag equilibrium:

$$\xi\,\frac{d\bar{v}_0}{d\xi} - \left(\frac{1 - \xi^2}{2}\right)\frac{d^2\bar{v}_0}{d\xi^2} + \bar{\Lambda}_2{}^2\,\frac{d^4\bar{v}_0}{d\xi^4} + \bar{\Lambda}_{12}\,\frac{d^4\bar{w}_0}{d\xi^4} - \bar{v}_0 = \bar{L}_{y0} \tag{28a}$$

$$\xi\,\frac{d\bar{w}_0}{d\xi} - \left(\frac{1 - \xi^2}{2}\right)\frac{d^2\bar{w}_0}{d\xi^2} + \bar{\Lambda}_{12}\,\frac{d^4\bar{v}_0}{d\xi^4} + \bar{\Lambda}_1{}^2\,\frac{d^4\bar{w}_0}{d\xi^4} = \bar{L}_{z0} - \beta_{pc}\xi \tag{28b}$$

The perturbation equations may also be reduced to two equations by making substitutions for the terms ϵ_0, $\Delta\epsilon$, Δu, and $\partial\Delta u/\partial\tau$. The perturbation strain is evaluated by integrating the perturbation radial force equation (26a).

$$\Delta\epsilon = \frac{2}{K}\int_{\epsilon}^{1} \frac{\partial\overline{\Delta v}}{\partial\tau}\, d\tau \tag{29}$$

Combining this equation with equation (26d) gives an expression for the perturbation radial displacement Δu in terms of flap and lead-lag displacements

$$\frac{\partial\Delta\bar{u}}{\partial\xi} = -\frac{d\bar{v}_0}{d\xi}\frac{\partial\Delta\bar{v}}{\partial\xi} - \frac{d\bar{w}_0}{d\xi}\frac{\partial\Delta\bar{w}}{\partial\xi} + \frac{2}{K}\int_{\xi}^{1} \frac{\partial\Delta\bar{v}}{\partial\tau}\, d\xi \tag{30}$$

The final term may be omitted because K is typically on the order of 10^2. This approximation is equivalent to the assumption that the beam is an inextensible member in terms of *perturbation* deflections. Integrating equation (30) then yields the perturbation radial displacement:

$$\Delta\bar{u} = -\int_{0}^{\xi}\left(\frac{d\bar{v}_0}{d\xi}\frac{\partial\Delta\bar{v}}{\partial\xi} + \frac{d\bar{w}_0}{d\xi}\frac{\partial\Delta\bar{w}}{\partial\xi}\right)d\xi \tag{31}$$

and

$$\frac{\partial\Delta\bar{u}}{\partial\tau} = -\frac{\partial}{\partial\tau}\int_{0}^{\xi}\left(\frac{d\bar{v}_0}{d\xi}\frac{\partial\Delta\bar{v}}{\partial\xi} + \frac{d\bar{w}_0}{d\xi}\frac{\partial\Delta\bar{w}}{\partial\xi}\right)d\xi \tag{32}$$

Equations (27), (29), and (32) may be substituted into equations (26b) and (26c) to obtain the final two perturbation equations in terms of the flap and lead-lag displacements Δw and Δv.

$$\xi\frac{\partial\Delta\bar{v}}{\partial\xi} - \left(\frac{1-\xi^2}{2}\right)\frac{\partial^2\Delta\bar{v}}{\partial\xi^2} + 2\frac{d\bar{v}_0}{d\xi}\frac{\partial\Delta\bar{v}}{\partial\tau} - 2\frac{d^2\bar{v}_0}{d\xi^2}\int_{\xi}^{1}\frac{\partial\Delta\bar{v}}{\partial\tau}\,d\xi + \bar{\Lambda}_2{}^2\frac{\partial^4\Delta\bar{v}}{\partial\xi^4} + \bar{\Lambda}_{12}\frac{\partial^4\Delta\bar{w}}{\partial\xi^4} + \frac{\partial^2\Delta\bar{v}}{\partial\tau^2}$$

$$-\Delta\bar{v} - 2\beta_{pc}\frac{\partial\Delta\bar{w}}{\partial\tau} - 2\frac{\partial}{\partial\tau}\int_{0}^{\xi}\left(\frac{d\bar{v}_0}{d\xi}\frac{\partial\Delta\bar{v}}{\partial\xi} + \frac{d\bar{w}_0}{d\xi}\frac{\partial\Delta\bar{w}}{\partial\xi}\right)d\xi = \Delta\bar{L}_y \tag{33a}$$

$$\xi \frac{\partial \Delta \bar{w}}{\partial \xi} - \left(\frac{1-\xi^2}{2}\right) \frac{\partial^2 \Delta \bar{w}}{\partial \xi^2} + 2 \frac{d\bar{w}_0}{d\xi} \frac{\partial \Delta \bar{v}}{\partial \tau} - 2 \frac{d^2 \bar{w}_0}{d\xi^2} \int_{\xi}^{1} \frac{\partial \Delta \bar{v}}{\partial \tau} d\xi + \bar{\Lambda}_{12} \frac{\partial^4 \Delta \bar{v}}{\partial \xi^4} + \bar{\Lambda}_1{}^2 \frac{\partial^4 \Delta \bar{w}}{\partial \xi^4} + \frac{\partial^2 \Delta \bar{w}}{\partial \tau^2}$$

$$+ 2\beta_{pc} \frac{\partial \Delta \bar{v}}{\partial \tau} = \Delta \bar{L}_z \qquad (33b)$$

The singly underlined portions of equations (33) represent the linearized Coriolis and centrifugal terms that result from retaining the nonlinearities noted above. They are necessary for a proper description of rotor blade dynamics because, in combination with aerodynamic forces, they can lead to flap-lag instability (refs. 1, 2). Other portions of the equations are doubly underlined; these are the elastic coupling terms which can be strongly stabilizing for the flap-lag motion (ref. 2).

Aerodynamic Forces

The aerodynamic forces per unit length denoted by L_y and L_z are the components perpendicular and parallel to the plane of rotation, and are related to the lift and drag forces of the rotor airfoil by the following.

$$L_y = -L \sin \varphi - D \cos \varphi \qquad (34)$$

$$L_z = L \cos \varphi - D \sin \varphi \qquad (35)$$

The angle φ defines the angle of the resultant instantaneous velocity vector V with respect to the plane of rotation. These parameters are illustrated in figure 3. The angle φ is defined by the two orthogonal components of V

$$\varphi \equiv \tan^{-1} \frac{U_P}{U_T} \qquad (36)$$

The equations for lift and drag based on quasi-steady, strip theory aerodynamics are

$$L \equiv \frac{1}{2} \rho_\infty a c V^2 \alpha \qquad (37)$$

$$D \equiv \frac{1}{2} \rho_\infty c V^2 c_{d_o} \qquad (38)$$

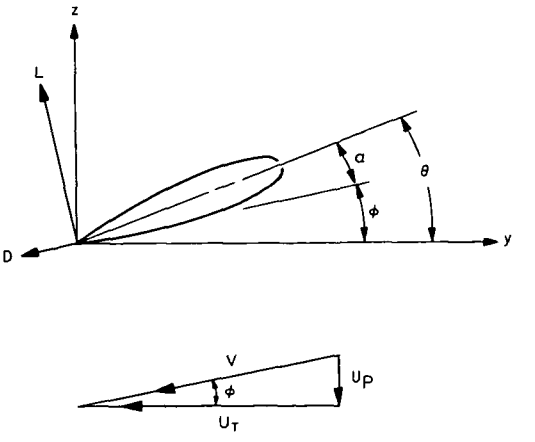

Figure 3.– Orientation of fluid velocity components and aerodynamic forces.

where the local section angle of attack is equal to

$$\alpha \equiv \theta - \varphi \tag{39}$$

Note that the local blade pitch angle θ is identical to the pitch angle imposed at the blade root since torsional elastic deformations are not treated. However, small geometric rotations of the blade section chord line due to combined flap and lead-lag bending are neglected. (Although these rotations are very small, they can become significant when blade pre-cone is present.) Combining equations (34) through (39) and using small angle approximations yields the following equations for the aerodynamic forces:

$$L_y = -\frac{1}{2}\rho_\infty acU_T^2\left[1+\left(\frac{U_P}{U_T}\right)^2\right]\left[\theta\,\frac{U_P}{U_T}-\left(\frac{U_P}{U_T}\right)^2+\frac{c_{d_o}}{a}\right] \tag{40}$$

$$L_z = \frac{1}{2}\rho_\infty acU_T^2\left[1+\left(\frac{U_P}{U_T}\right)^2\right]\left[\theta-\frac{U_P}{U_T}-\frac{c_{d_o}}{a}\,\frac{U_P}{U_T}\right] \tag{41}$$

The components of V are given by

$$U_P = v_i + \frac{\partial w}{\partial t} \tag{42}$$

$$U_T = \Omega x + \frac{\partial v}{\partial t} \tag{43}$$

where v_i is the induced velocity of the rotor. A reasonably accurate equation for the induced velocity of a hovering rotor can be obtained from blade-element momentum theory (ref. 4). Approximating the induced velocity as constant over the entire area of the disc, equal to the value at $\xi = 3/4$, we obtain:

$$\frac{v_i}{\Omega R} = \frac{\pi\sigma}{8}\left(\sqrt{1+\frac{12}{\pi\sigma}|\theta|}-1\right) \tag{44}$$

After noting that $(U_P/U_T)^2 \ll 1$ and $c_{d_o}/a \ll 1$, the dimensionless relations for the aerodynamic forces become

$$\bar{L}_y = -\frac{\gamma}{6}\left[\theta\xi\bar{v}_i - \bar{v}_i^2 + \frac{c_{d_o}}{a}\,\xi^2 + \left(\theta\bar{v}_i + 2\xi\frac{c_{d_o}}{a}\right)\frac{\partial\bar{v}}{\partial\tau} + (\theta\xi - 2\bar{v}_i)\,\frac{\partial\bar{w}}{\partial\tau}\right] \tag{45}$$

$$\bar{L}_z = \frac{\gamma}{6}\left[\theta\xi^2 - \xi\bar{v}_i + (2\theta\xi - \bar{v}_i)\,\frac{\partial\bar{v}}{\partial\tau} - \xi\,\frac{\partial\bar{w}}{\partial\tau}\right] \tag{46}$$

The equilibrium and perturbation components of the aerodynamic forces to be used in equations (28) and (33) can be obtained from equations (45) and (46) and are

$$\bar{L}_{y_0} = \frac{\gamma}{6}\left(\bar{v}_i^2 - \frac{c_{d_O}}{a}\,\xi^2 - \theta\xi\bar{v}_i\right) \tag{47a}$$

$$\bar{L}_{z_0} = \frac{\gamma}{6}\left(\theta\xi^2 - \xi\bar{v}_i\right) \tag{47b}$$

$$\Delta\bar{L}_y = -\frac{\gamma}{6}\left[\left(\theta\bar{v}_i + 2\xi\,\frac{c_{d_O}}{a}\right)\frac{\partial\Delta\bar{v}}{\partial\tau} + (\theta\xi - 2\bar{v}_i)\,\frac{\partial\Delta\bar{w}}{\partial\tau}\right] \tag{48a}$$

$$\Delta\bar{L}_z = -\frac{\gamma}{6}\left[(\bar{v}_i - 2\theta\xi)\,\frac{\partial\Delta\bar{v}}{\partial\tau} + \xi\,\frac{\partial\Delta\bar{w}}{\partial\tau}\right] \tag{48b}$$

Final Equations

Combining equations (28) and (47) yields the final equilibrium equations

$$\xi\,\frac{d\bar{v}_0}{d\xi} - \left(\frac{1-\xi^2}{2}\right)\frac{d^2\bar{v}_0}{d\xi^2} + \bar{\Lambda}_2{}^2\,\frac{d^4\bar{v}_0}{d\xi^4} + \bar{\Lambda}_{12}\,\frac{d^4\bar{w}_0}{d\xi^4} - \bar{v}_0 = \frac{\gamma}{6}\left(\bar{v}_i^2 - \frac{c_{d_O}}{a}\,\xi^2 - \theta\xi\bar{v}_i\right) \tag{49a}$$

$$\xi\,\frac{d\bar{w}_0}{d\xi} - \left(\frac{1-\xi^2}{2}\right)\frac{d^2\bar{w}_0}{d\xi^2} + \bar{\Lambda}_{12}\,\frac{d^4\bar{v}_0}{d\xi^4} + \bar{\Lambda}_1{}^2\,\frac{d^4\bar{w}_0}{d\xi^4} = \frac{\gamma}{6}\,(\theta\xi^2 - \xi\bar{v}_i) - \beta_{pc}\xi \tag{49b}$$

The final perturbation equations obtained from equations (33) and (48) are

$$\xi\,\frac{\partial\Delta\bar{v}}{\partial\xi} - \left(\frac{1-\xi^2}{2}\right)\frac{\partial^2\Delta\bar{v}}{\partial\xi^2} + \frac{2d\bar{v}_0}{d\xi}\,\frac{\partial\Delta v}{\partial\tau} - \frac{2d^2\bar{v}_0}{d\xi^2}\int_\xi^1 \frac{\partial\Delta\bar{v}}{\partial\tau}\,d\xi + \bar{\Lambda}_2{}^2\,\frac{\partial^4\Delta\bar{v}}{\partial\xi^4} + \bar{\Lambda}_{12}\,\frac{\partial^4\Delta\bar{w}}{\partial\xi^4} + \frac{\partial^2\Delta\bar{v}}{\partial\tau^2}$$

$$- \Delta\bar{v} - 2\beta_{pc}\,\frac{\partial\Delta\bar{w}}{\partial\tau} - 2\,\frac{\partial}{\partial\tau}\int_0^\xi\left(\frac{d\bar{v}_0}{d\xi}\,\frac{\partial\Delta\bar{v}}{\partial\xi} + \frac{d\bar{w}_0}{d\xi}\,\frac{\partial\Delta\bar{w}}{\partial\xi}\right)d\xi + \frac{\gamma}{6}\left[\left(\theta\bar{v}_i + 2\xi\,\frac{c_{d_O}}{a}\right)\frac{\partial\Delta\bar{v}}{\partial\tau}\right.$$

$$\left. + (\theta\xi - 2\bar{v}_i)\,\frac{\partial\Delta\bar{w}}{\partial\tau}\right] = 0 \tag{50a}$$

$$\xi \frac{\partial \Delta\bar{w}}{\partial \xi} - \left(\frac{1-\xi^2}{2}\right) \frac{\partial^2 \Delta\bar{w}}{\partial \xi} + \frac{2d\bar{w}_0}{d\xi} \frac{\partial \Delta\bar{v}}{\partial \tau} - \frac{2d^2\bar{w}_0}{d\xi^2} \int_{\xi}^{1} \frac{\partial \Delta\bar{v}}{\partial \tau} \, d\xi + \bar{\Lambda}_{12} \frac{\partial^4 \Delta\bar{v}}{\partial \xi^4} + \bar{\Lambda}_1{}^2 \frac{\partial^4 \Delta\bar{w}}{\partial \xi^4} + \frac{\partial^2 \Delta\bar{w}}{\partial \tau^2}$$

$$+ 2\beta_{pc} \frac{\partial \Delta\bar{v}}{\partial \tau} + \frac{\gamma}{6}\left[(v_i - 2\theta\xi) \frac{\partial \Delta\bar{v}}{\partial \tau} + \xi \frac{\partial \Delta\bar{w}}{\partial \tau}\right] = 0 \qquad (50b)$$

Solution of Equations of Motion

The flap-lag equations that have been developed can be further simplified using Galerkin's method. The nonhomogeneous equilibrium equations are linear, variable coefficient, ordinary differential equations for $\bar{v}_0(\xi)$ and $\bar{w}_0(\xi)$. The homogeneous perturbation equations are linear, variable coefficient integro-partial differential equations for $\Delta\bar{v}(\xi,\tau)$ and $\Delta\bar{w}(\xi,\tau)$. The coefficients of the perturbation equations are also functions of the equilibrium displacements $\bar{v}_0$, $\bar{w}_0$ as a consequence of the nonlinearity of the original equations of motion. For Galerkin's method we assume an approximate series solution in terms of the elastic bending modes $\varphi_j(\xi)$

$$\left.\begin{aligned} \bar{v}_0 &= \sum_{j=1}^{N} \zeta_{0_j} \varphi_j(\xi) \\ \bar{w}_0 &= \sum_{j=1}^{N} \beta_{0_j} \varphi_j(\xi) \\ \Delta\bar{v} &= \sum_{j=1}^{N} \Delta\zeta_j(\tau) \varphi_j(\xi) \\ \Delta\bar{w} &= \sum_{j=1}^{N} \Delta\beta_j(\tau) \varphi_j(\xi) \end{aligned}\right\} \qquad (51)$$

These series expressions are substituted in equations (49) and (50), which are multiplied in turn by each bending mode function $\varphi_i(\xi)$ and integrated along the length of the beam from $\xi = 0$ to 1. This procedure reduces the equilibrium equations to $2N$ linear algebraic equations for ζ_{0_j} and

β_{O_j}, and the perturbation equations to $2N$ linear constant coefficient ordinary differential equations for $\Delta\zeta_j(\xi)$ and $\Delta\beta_j(\xi)$. The integrals involving various combinations and derivatives of $\varphi_j(\zeta)$ are the Galerkin integrals. The equation for the bending modes used to evaluate these integrals is

$$\varphi_j(\xi) = \cosh(\omega_j\xi) - \cos(\omega_j\xi) - f_j[\sinh(\omega_j\xi) - \sin(\omega_j\xi)] \tag{52}$$

This is the equation for the modes of a nonrotating uniform cantilever beam, and the constants ω_j and f_j available in reference 5 are given in table 1. The Galerkin integrals are evaluated exactly, where possible, according to the tabulated integrals of reference 6. Otherwise they are evaluated by numerical integration.

TABLE 1.– CONSTANTS FOR NONROTATING CANTILEVERED BEAM BENDING MODES

j	ω_j	f_j
1	1.875104068712	0.7340955137589
2	4.694091132974	1.018467318759
3	7.854757438238	.9992244965174
4	10.99554073488	1.000033553252
5	14.13716839105	.9999985501087

The equilibrium and perturbation equations are then

$$\sum_{j=1}^{N}\left\{\zeta_{O_j}[D_{ij} + (\bar{\Lambda}_2{}^2\omega_j{}^4 - 1)\delta_{ij}] + \beta_{O_j}(\bar{\Lambda}_{12}\omega_j{}^4\delta_{ij})\right\} = \frac{\gamma}{6}\left(v_i{}^2A_i - v_i\theta B_i - \frac{c_{d_O}}{a}C_i\right) \tag{53a}$$

$$\sum_{j=1}^{N}[\zeta_{O_j}(\bar{\Lambda}_{12}\omega_j{}^4\delta_{ij}) + \beta_{O_j}(D_{ij} + \bar{\Lambda}_1{}^2\omega_j{}^4\delta_{ij})] = \frac{\gamma}{6}(\theta C_i - v_iB_i) - \beta_{pc}B_i \tag{53b}$$

$$\sum_{j=1}^{N}\left\{\Delta\ddot{\zeta}_j(\delta_{ij}) + \Delta\dot{\zeta}_j\left[2S_{ij} + \frac{\gamma}{6}\left(2\frac{c_{d_O}}{a}E_{i_j} + \theta v_i\delta_{ij}\right)\right] + \Delta\dot{\beta}_j\left[-2\beta_{pc}\delta_{ij} - 2T_{ij} + \frac{\gamma}{6}(\theta E_{ij} - 2v_i\delta_{ij})\right]\right.$$

$$\left. + \Delta\zeta_j[D_{ij} + (\bar{\Lambda}_2{}^2\omega_j{}^4 - 1)\delta_{ij}] + \Delta\beta_j(\bar{\Lambda}_{12}\omega_j{}^4\delta_{ij})\right\} = 0 \tag{54a}$$

$$\sum_{j=1}^{N}\Bigg\{\Delta\ddot{\beta}_j(\delta_{ij}) + \Delta\dot{\xi}_j\left[2\beta_{pc}\delta_{ij} + 2T_{ji} + \frac{\gamma}{6}\,(\bar{\nu}_i\delta_{ij} - 2\theta E_{ij})\right] + \Delta\dot{\beta}_j\left(-\frac{\gamma}{6}\,E_{ij}\right) + \Delta\zeta_j(\bar{\Lambda}_{1\,2}\,\bar{\omega}_j^{\,4}\,\delta_{ij})$$

$$+ \Delta\beta_j(D_{ij} + \bar{\Lambda}_1{}^2\,\omega_j^{\,4}\,\delta_{ij})\Bigg\} = 0 \qquad i = 1, 2, \ldots, N \tag{54b}$$

where the Galerkin integrals are

$$A_i = \int_0^1 \varphi_i \, d\xi = \frac{2f_i}{\omega_i} \tag{55a}$$

$$B_i = \int_0^1 \xi\varphi_i \, d\xi = \frac{2}{\omega_i{}^2} \tag{55b}$$

$$C_i = \int_0^1 \xi^2\varphi_i \, d\xi = 4(-1)^{i+1}\,\frac{f_i}{\omega_i{}^3} \tag{55c}$$

$$D_{ij} = \int_0^1 \xi\varphi_i\varphi_j' - \int_0^1 \left(\frac{1-\xi^2}{2}\right)\varphi_i\varphi_j'' \, d\xi = \int_0^1 \left(\frac{1-\xi^2}{2}\right)\varphi_i'\varphi_j' \, d\xi \tag{55d}$$

$$E_{ij} = \int_0^1 \xi\varphi_i\varphi_j \, d\xi \tag{55e}$$

$$F_{ijk} = \frac{1}{\omega_k{}^4}\int_0^1 \varphi_i\varphi_j''\varphi_k''' \, d\xi + \int_0^1 \varphi_i\varphi_j'\varphi_k \, d\xi = -\frac{1}{\omega_k{}^4}\int_0^1 \varphi_i'\varphi_j'\varphi_k''' \, d\xi \tag{55f}$$

$$\left(\text{note } \int_0^1 \varphi_i \int_0^\xi \varphi_j'\varphi_k' \, d\xi = -\frac{1}{\omega_i{}^4}\int_0^1 \varphi_i'''\varphi_j'\varphi_k' \, d\xi = F_{kji}\right)$$

and where

$$S_{ij} = \sum_{k=1}^{N} (F_{ikj} - F_{jki})\zeta_{ok} \tag{56a}$$

$$T_{ij} = \sum_{k=1}^{N} F_{jki}\beta_{ok} \tag{56b}$$

These equations are solved using standard methods. The equilibrium displacements are used to determine the coefficients of the perturbation equations, which are then solved for eigenvalues and thus the stability characteristics of interest.

RESULTS AND DISCUSSION

Uncoupled Natural Frequencies

When the aerodynamic terms in the rotor blade equations are eliminated, the resulting perturbation solutions provide the rotating natural frequencies of the rotor blade motion. For untwisted blades at zero pitch angle, the equations for the flap and lead-lag degrees of freedom are independent, and the solutions yield the uncoupled natural frequencies.

The first two flap and first two lead-lag uncoupled rotating frequencies of typical hingeless rotor blades are given in figure 4. Two examples are shown, one a soft inplane configuration and the other stiff inplane. The terms soft or stiff inplane refer, respectively, to rotor blades with first rotating lead-lag frequencies less than or greater than the nominal rotational frequency of the rotor. These results, using three bending modes for both the flap and lead-lag degrees of freedom, illustrate typical variations of the rotating frequencies with the rotor angular velocity Ω. The frequencies and angular velocity are made dimensionless by a nominal angular velocity Ω_o, which can be interpreted as the normal rotational velocity of the rotor. The dimensionless bending stiffness of the rotor blade is inversely proportional to the rotational speed, $K = K_o/(\Omega/\Omega_o)^2$ where $K_o = EA/m\Omega_o{}^2R^2$.

The convergence of the solution with the number of bending modes is shown in figure 5. Here, the rotating frequencies are shown as a function of the nonrotating frequencies. They are both made dimensionless by the rotor angular velocity. The use of this nondimensional parameter is a means of distinguishing between different rotor blade configurations. For a given rotor speed, then, the nonrotating frequency is a measure of the bending stiffness of the rotor blade. The first flap and lead-lag frequencies are of primary interest here and the results show that convergence is quite good for rotor blades of high bending stiffness (or low angular velocity) but becomes poor for low stiffness (or high angular velocity). To give proper perspective to these results, we must consider them in the light of typical blade frequency values. For the lead-lag degree of freedom, a typical stiff inplane hingeless rotor blade would have $\bar{\omega}_\zeta \sim 1.5$, and a single bending mode would accurately define the rotating lead-lag frequency. For a soft inplane configuration, $\bar{\omega}_\zeta \sim 0.7$, two bending modes would be required.

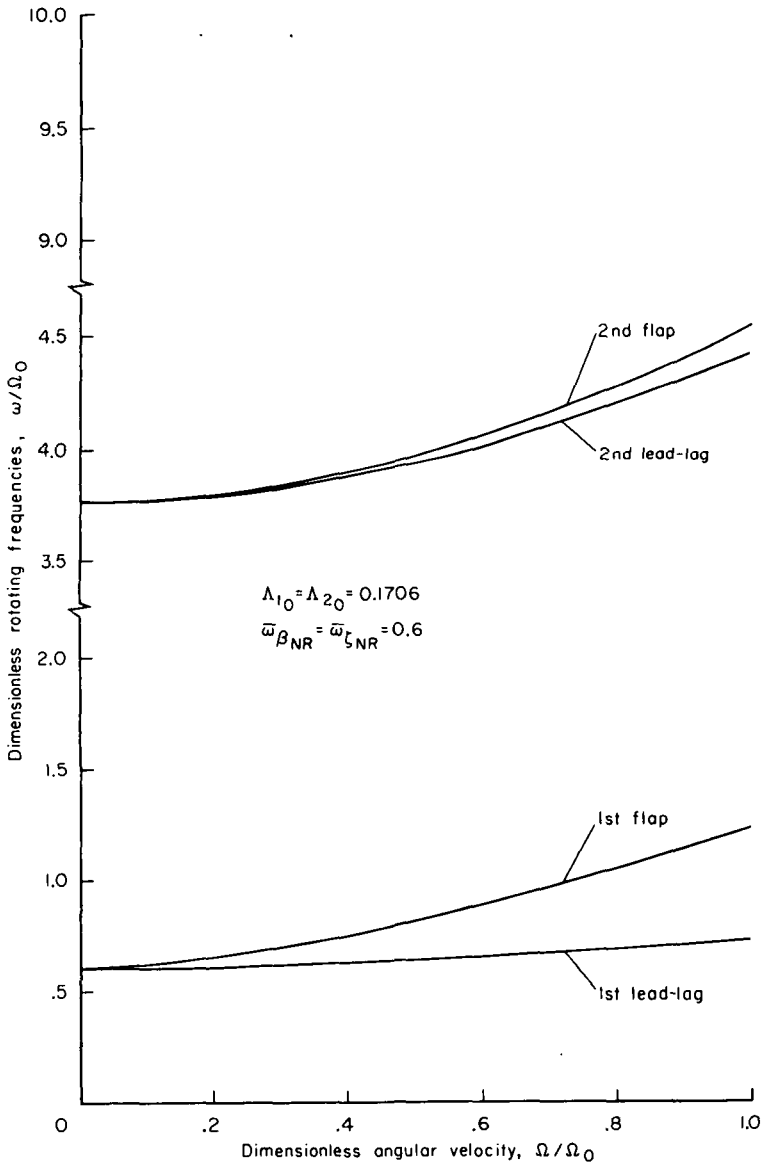

(a) Soft inplane configuration.

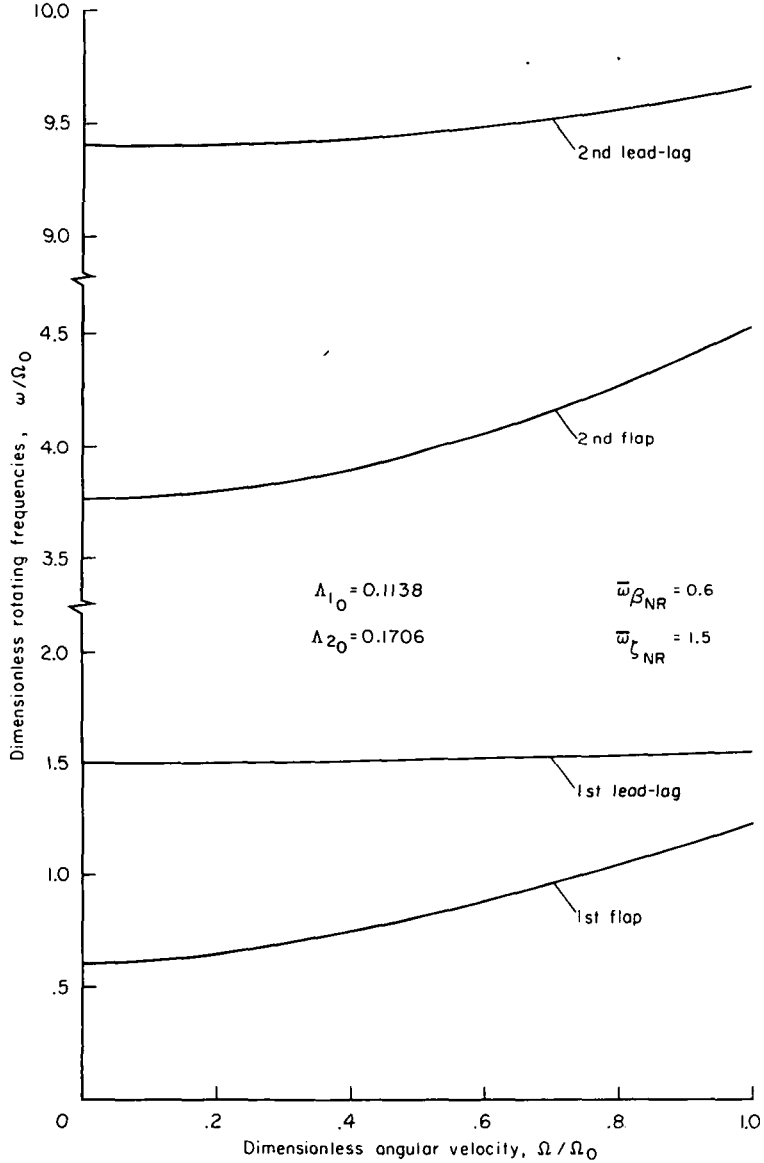

(b) Stiff inplane configuration.

Figure 4.– Variation of the first two uncoupled rotating natural frequencies with rotor angular velocity $\theta = 0$.

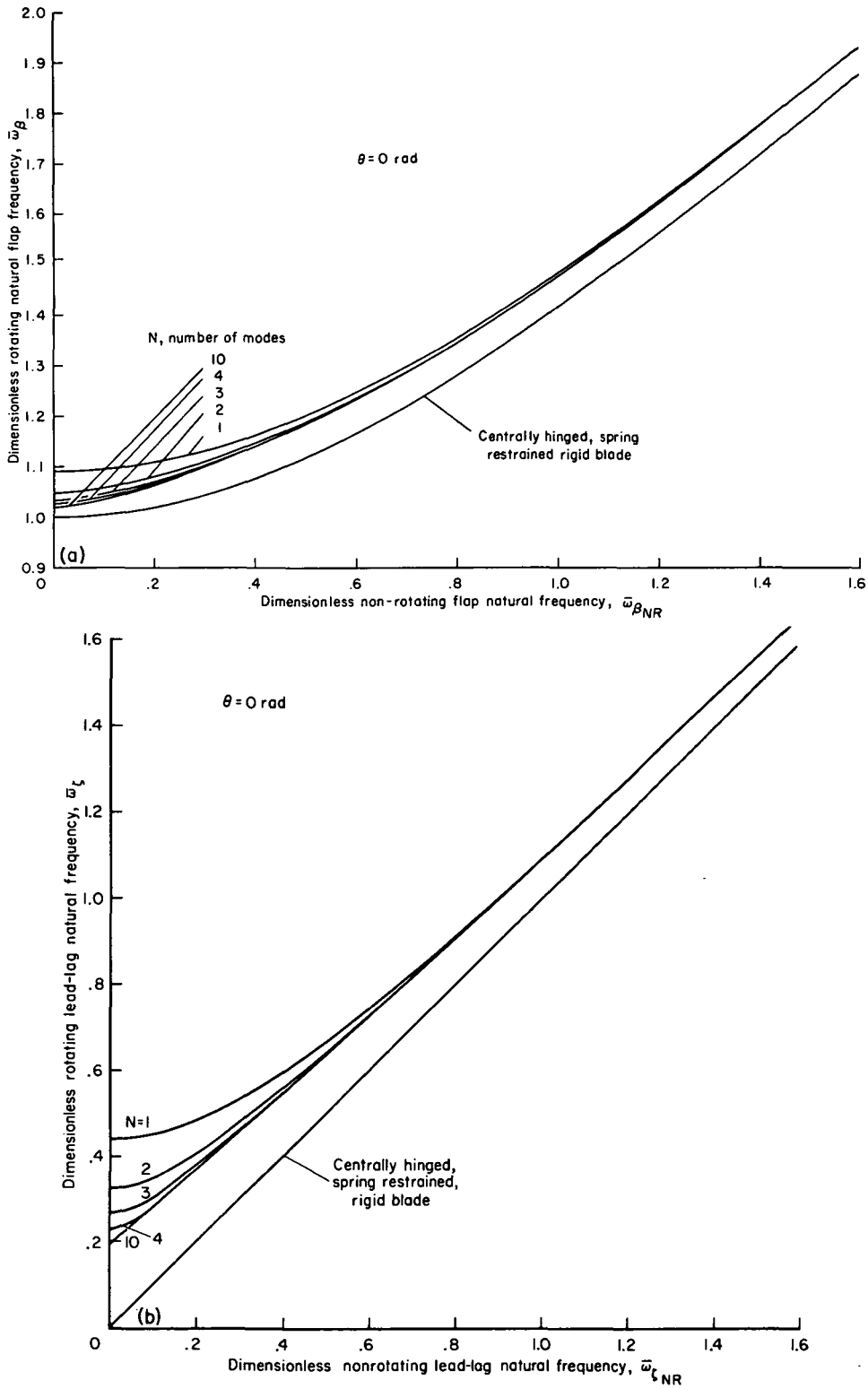

(a) First flap bending mode.
(b) First lead-lag bending mode.

Figure 5.– Effect of number of modes on the uncoupled rotating natural frequencies.

For the flapping degree of freedom, a typical first bending mode frequency would be $\bar{\omega}_\beta \sim 1.1$, which would require at least two bending modes. This is particularly important for hingeless rotors because the flapping response characteristics can be sensitive to small changes in the first flap mode frequency.

It should be noted that the convergence characteristics in figure 5 are directly related to the use of the simple nonrotating uniform cantilever beam mode shapes and can be viewed as a measure of the usefulness of approximate modes. However, for use in the stability analyses reported herein, the use of nonrotating beam modes simplifies the parametric studies because different mode shapes are not required for different rotor blade stiffness values.

Also shown for comparison in figure 5 are the rotating frequencies obtained using the approximate centrally hinged, spring restrained, rigid blade representation. The uncoupled flap and lead-lag natural frequencies are given by the following relations (ref. 2):

$$\bar{\omega}_\beta = \sqrt{1 + \bar{\omega}^2_{\beta_{NR}}} \tag{57a}$$

$$\bar{\omega}_\zeta = \bar{\omega}_{\zeta_{NR}} \tag{57b}$$

In effect, these frequencies are a special result for the case of linear mode shapes for the flap and lead-lag bending deflections. These modes might be expected to yield the correct first rotating frequencies in the limiting case of vanishing blade bending stiffness because the mode shape approaches a straight line. It must be noted, however, that because of the condition of zero slope at the root of the cantilevered blade a linear mode shape is invalid at that point.

Stability Characteristics

The dynamic stability characteristics of the flap and lead-lag bending oscillations of elastic hingeless rotor blades without pre-cone in a hovering flight condition is shown in figure 6. The results are presented in locus of root form for both the first flap and lead-lag modes as the blade pitch angle is increased from zero. Loci for several configurations having various lead-lag stiffnesses are presented. As discussed above, only the soft and stiff inplane configurations are representative of actual hingeless rotors. The other parameters are chosen to be representative.

The flap mode is typically well damped. The lead-lag damping is substantially increased for higher pitch angles with no indication of instability. This is consistent with earlier findings of reference 2 for the rigid blade model with the appropriate elastic coupling characteristics. In effect, the elastic flap-lag coupling introduces the large flap mode damping into the lead-lag mode, thereby augmenting the small inherent lead-lag damping and nullifying the destabilizing inertial and aerodynamic flap-lag coupling effects.

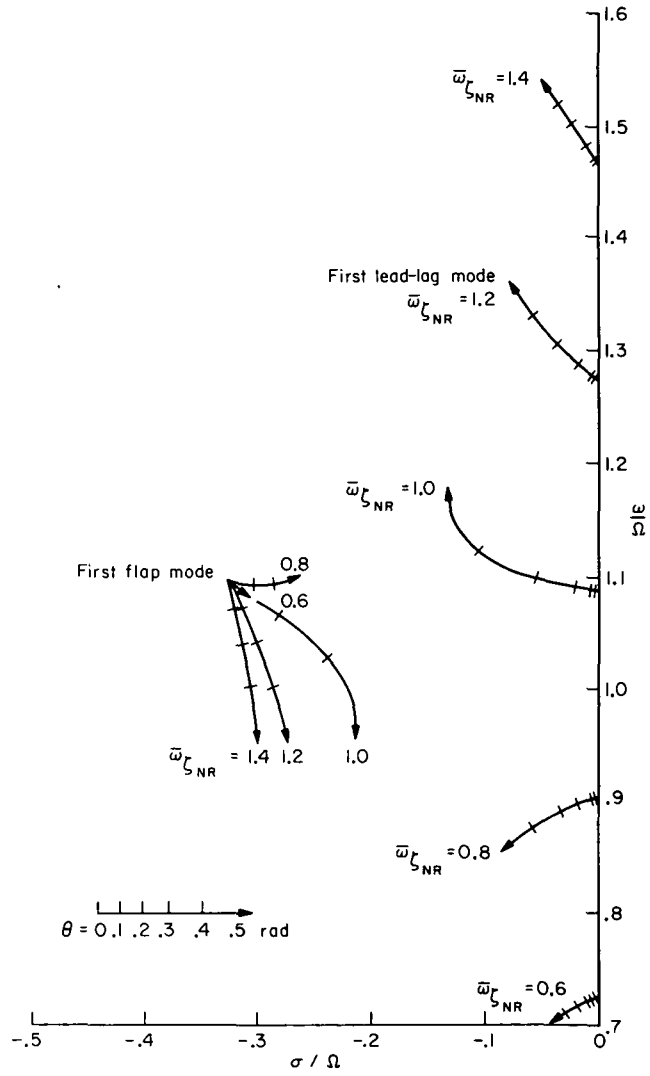

Figure 6.– Locus of roots with increasing pitch angle, $\gamma = 5.0$, $\sigma = 0.05$, $\bar{\omega}_{\beta_{NR}} = 0.6$, $c_{d_o} = 0.01$, N = 3.

A comparison between the results of the elastic blade and the rigid blade model will now be made. A schematic picture of the approximate centrally hinged, spring restrained, rigid blade is given in figure 7. The orientation of the flap and lead-lag restraint springs (parallel and perpendicular to the blade chord line, respectively) simulates the elastic coupling characteristics of the actual elastic blade. The spring stiffnesses are chosen so that the uncoupled rotating flap and lead-lag natural frequencies match the corresponding first mode rotating natural frequencies of the elastic blade. The roots for the rigid blade configuration are shown in figure 8, and they exhibit behavior nearly

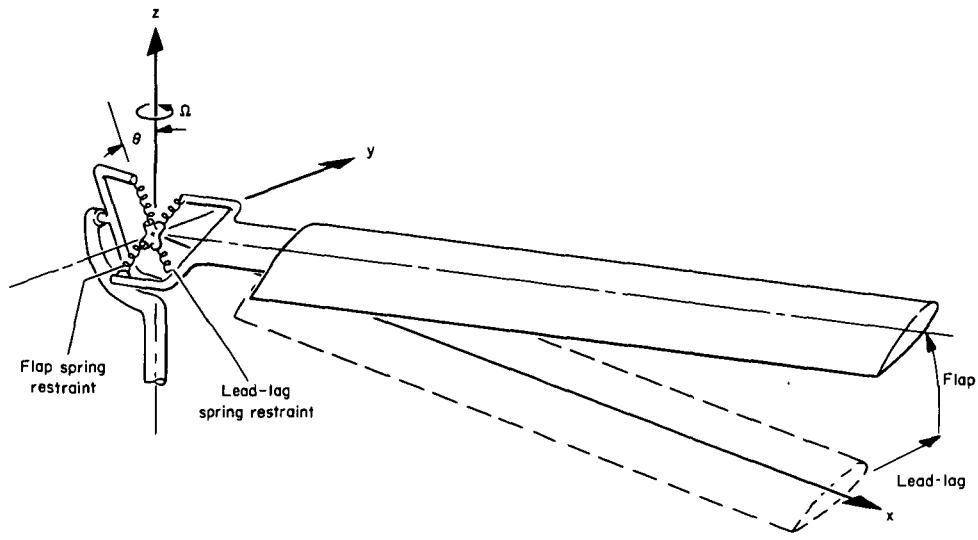

Figure 7.– Schematic of approximate centrally hinged, spring restrained, rigid blade representation with springs oriented to match the elastic coupling of elastic rotor blades.

identical to the elastic blade results discussed above. The differences are a reduction in flap mode damping and a small reduction in the stiff inplane lead-lag damping for the rigid blade representation. The significance of the close agreement is that the mode shape does not play a large role in the flap-lag stability characteristics, at least in the hover condition, and the simple rigid blade model should be quite adequate for approximate stability analyses if the equivalent spring constants are chosen as discussed above.

Although the results just presented confirm the relatively small effect of mode shape on stability, it is of interest to examine the sensitivity of the elastic blade stability to the number of flap and lead-lag bending modes included in the solution. The roots in figure 6 were computed using three bending modes for each degree of freedom; we will now investigate the effect of using only one or two modes. Since the first lead-lag mode damping is of most interest, we will consider only the real part of this root. Before presenting the results it should be noted that there are two ways of making the comparisons. This depends on whether the rotating or nonrotating first mode bending frequency is considered to be the independent parameter defining the rotor blade configuration. If one uses the rotating frequency as the independent parameter, as for the rigid blade comparison, the nonrotating frequency, or blade stiffness parameter K, will depend on the number of bending modes used. The particular variation can be obtained from figure 4. In this case the effect of the number of bending modes on lead-lag damping will be primarily due to coupling between the various bending modes. Alternatively, if the blade stiffness parameter K or the nonrotating frequency is chosen as the independent parameter, variations in the number of bending modes will directly influence the rotating first mode frequency. This would introduce an additional effect, since the lead-lag damping is influenced by the proximity of the flap and lead-lag rotating frequencies.

The comparisons of first-lead lag mode damping are given in table 2 for a soft and a stiff inplane rotor blade configuration operating at a pitch angle of 0.3 rad. The sensitivity of damping to the number of modes is quite small but certain trends are discernible. As expected, holding the rotating natural frequencies constant minimized the effect of modal interaction, in contrast to holding the

TABLE 2.– EFFECT OF NUMBER OF FLAP AND LEAD-LAG BENDING MODES ON THE FIRST LEAD-LAG MODE DAMPING AT $\theta = 0.3$, $\bar{\omega}_{\beta_{NR}} = 0.4$.

Soft inplane configuration, $\bar{\omega}_{\zeta_{NR}} = 0.6$			Stiff inplane configuration, $\bar{\omega}_{\zeta_{NR}} = 1.4$		
N	$-\sigma_\zeta/\Omega$		N	$-\sigma_\zeta/\Omega$	
3	0.01689		3	0.02342	
	$\bar{\omega}_{\zeta_{NR}}$ const	$\bar{\omega}_\zeta$ const		$\bar{\omega}_{\zeta_{NR}}$ const	$\bar{\omega}_\zeta$ const
2	0.01663	0.01694	2	0.02352	0.02344
1	.01567	.01714	1	.02390	.02363
Rigid	---	.01713	Rigid	---	.02253

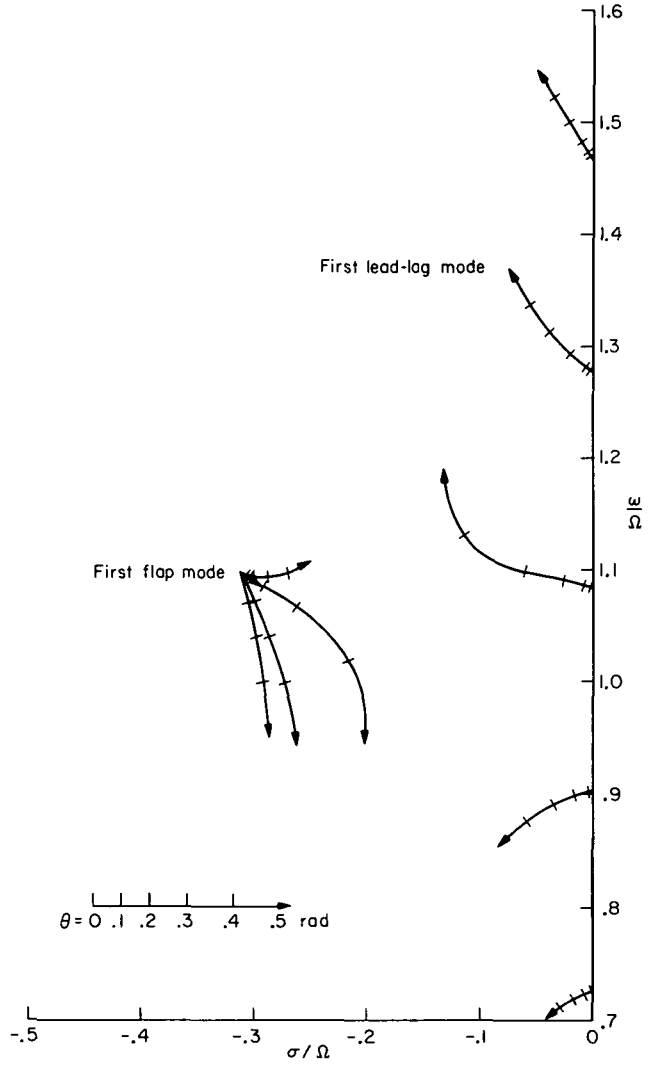

Figure 8.– Locus of roots with increasing pitch angle for rigid blade representation. Rotating natural frequencies are chosen to match the corresponding results in figure 6.

nonrotating frequencies constant. Furthermore, the effect of number of modes was more evident for the soft inplane configuration, which is consistent with the earlier results. This can be attributed to the increasing disparity between nonrotating and rotating mode shapes as the stiffness is reduced. For completeness, the table includes results presented graphically in figure 8 for the approximate rigid blade. It is interesting to note that the rigid blade is as accurate as the single mode solution for the soft inplane configuration, but underestimates the damping for the stiff configuration. Results for the rigid blade for the case of constant nonrotating frequency are not presented because of the unrealistic frequencies of this approximate representation.

These results indicate that the basic character of flap-lag stability is little changed by using the approximate rigid blade (with the proper rotating natural frequencies) or a single mode representation for the elastic bending deflections. A small degradation in the accuracy of the lead-lag damping can result from the rigid blade approximation, but a single bending mode gives quite reasonable accuracy.

The nonlinear Coriolis and centrifugal terms in the equations discussed above were considered essential to properly describe

the flap-lag stability characteristics of elastic blades. Although the above results indicate that the destabilizing aerodynamic and inertial coupling is more than compensated for by the elastic coupling of a rotating uniform beam, the destabilizing nonlinear terms are also of interest for their influence on the lead-lag damping. This is shown in figure 9, again for two rotor blade configurations. The nonlinear terms do act to destabilize the lead-lag degree of freedom and their effect is substantial. For rotating beam configurations with radially nonuniform stiffness distributions, reference 2 implies that the elastic coupling may not, in general, prevent flap-lag instability, and the nonlinear inertial terms will then determine the rotor blade stability characteristics. This problem, however, is beyond the scope of the present report.

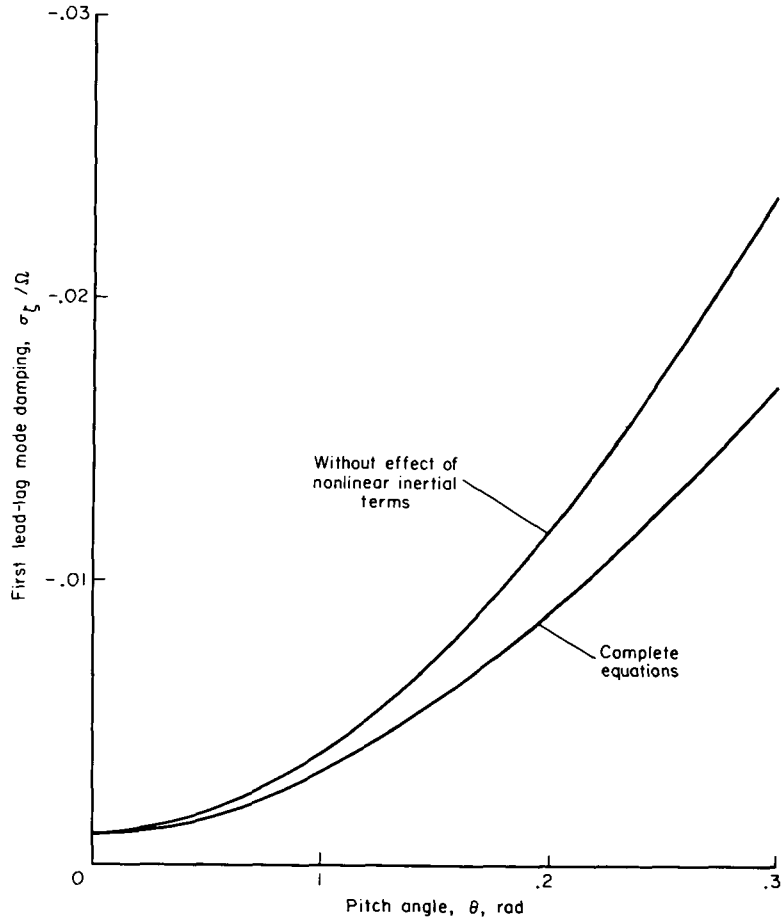

(a) Soft inplane configuration, $\bar{\omega}_{\zeta_{NR}} = 0.6$.

Figure 9.– Effect of the nonlinear inertial terms on the lead-lag mode damping, $\gamma = 5.0, \sigma = 0.05, \bar{\omega}_{\beta_{NR}} = 0.6, c_{d_0} = 0.01, N = 3$.

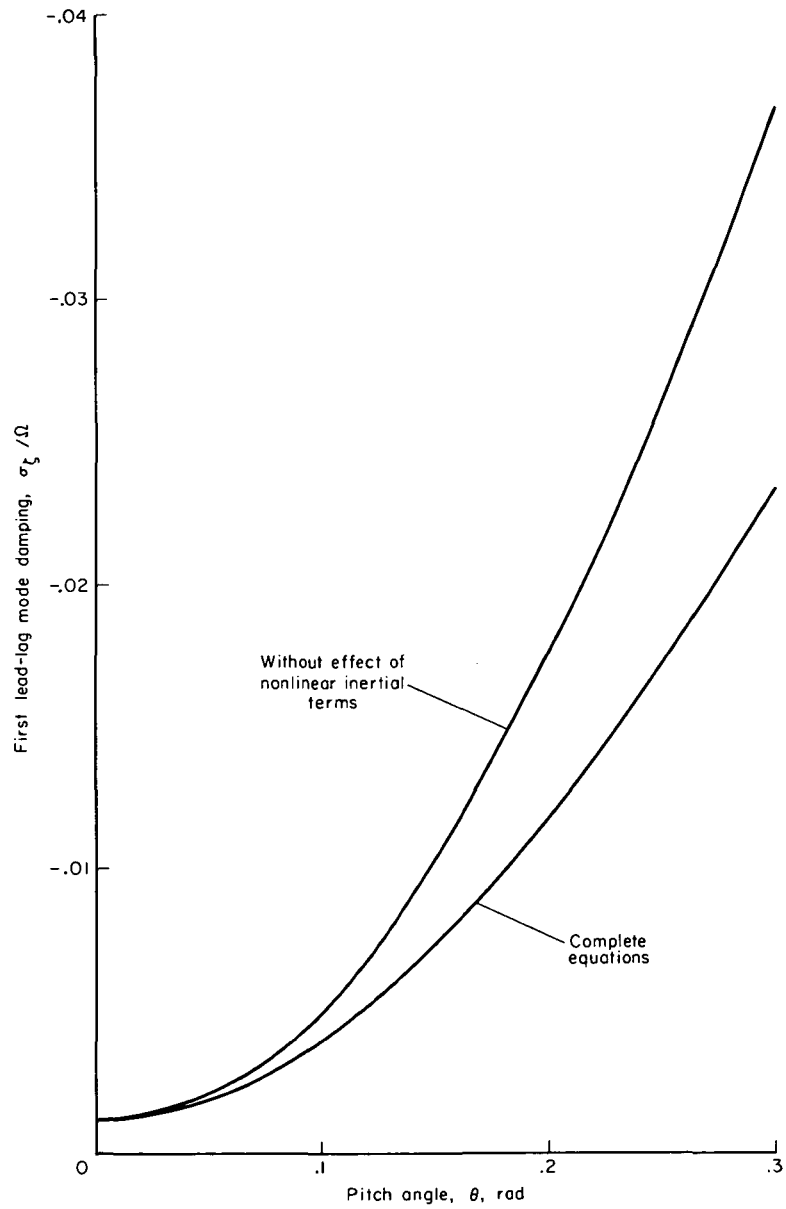

(b) Stiff inplane configuration, $\bar{\omega}_{\zeta_{NR}} = 1.4$.

Figure 9.– Concluded.

Rotor blade pre-cone is an important design parameter for hingeless rotors and previous analyses (refs. 1 and 2) with the approximate rigid blade representation indicate that it has a substantial effect on flap-lag stability. Some representative results for the lead-lag damping of the elastic blade are shown in figures 10(a) and 10(b) for the soft and stiff inplane configurations, respectively. In general, either positive or negative pre-cone is stabilizing, except for small positive increments with the stiff inplane configuration.

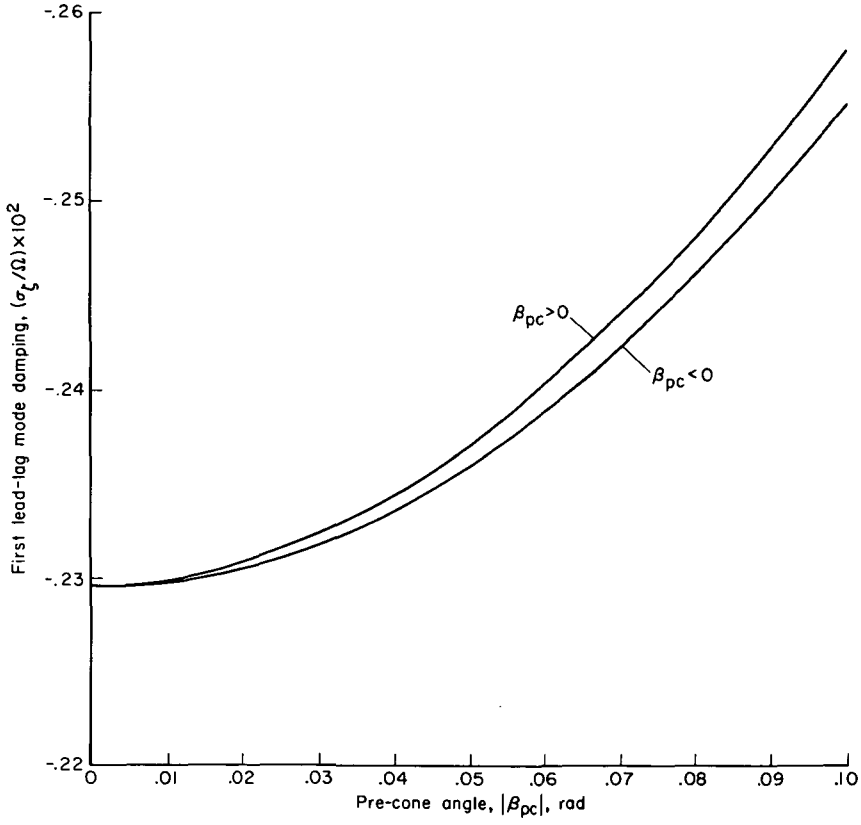

(a) Soft inplane configuration, $\bar{\omega}_{\zeta_{NR}}$ =0.6.

Figure 10.– Effect of pre-cone on the lead-lag mode damping, $\gamma = 5.0$, $\sigma = 0.05, \bar{\omega}_{\beta_{NR}} = 0.6, c_{d_o} = 0.01$, N = 1, $\theta = 0.1$.

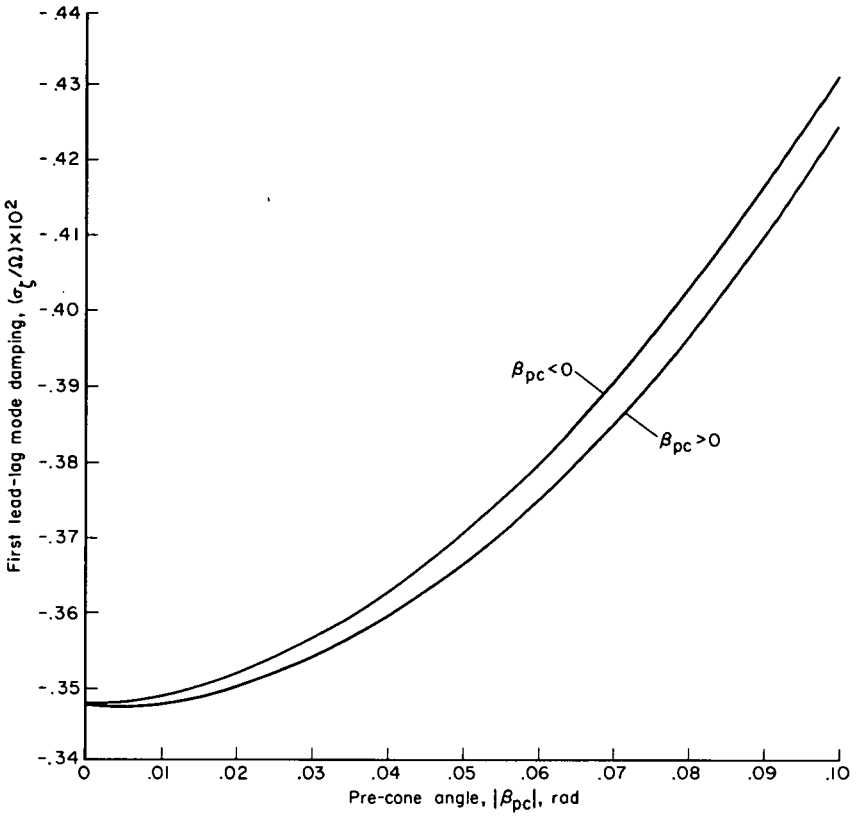

(b) Stiff inplane configuration, $\bar{\omega}_{\zeta_{NR}} = 1.5$.

Figure 10.– Concluded.

The effects of rotary inertia terms in the rotating beam equations were determined to be of nearly negligible magnitude. This was checked with the numerical results by computing the lead-lag mode damping both with and without the rotary inertia terms. The results are given in table 3 and confirm the negligible effect on flap-lag stability.

TABLE 3.– EFFECT OF ROTARY INERTIA ON THE FIRST LEAD-LAG MODE DAMPING, $\bar{\omega}_{\beta_{NR}} = 0.6$, $\bar{\omega}_{\zeta_{NR}} = 1.5$, $\gamma = 5.0$, $c_{d_o} = 0.01$, $\sigma = 0.05$, $\theta = 0.3$, N = 1

$-\sigma_\zeta/\Omega$	
No rotary inertia	With rotary inertia
0.021199	0.021190

CONCLUDING REMARKS

1. Conventional linear equations of motion cannot be used to determine the stability of coupled flap and lead-lag degrees of freedom of cantilevered, torsionally rigid, elastic rotor blades. An additional equation for the radial degree of freedom and a nonlinear strain-displacement relation are required. The basic nonlinear flap-lag equations can be linearized about a suitable equilibrium condition and still retain the effect of the important inertial flap-lag coupling terms. The calculation of lead-lag damping was shown to be very much a function of these terms.

2. Flap-lag oscillations in hover for untwisted blades of uniform mass and stiffness were found to be stable over a wide range of parameters. It was determined that the effects of elastic flap-lag coupling introduced sufficient flap mode aerodynamic damping into the weakly damped lead-lag mode to overcome the destabilizing inertial coupling. Previous results (ref. 2) for an approximate, centrally hinged, spring restrained, rigid blade representation, however, indicate that this effect can be reduced for elastic blades with twist and/or nonuniform mass and stiffness.

3. The first mode frequency and damping for the elastic blade motions were found to be nearly identical to results obtained with the rigid blade representation provided that the rotating natural frequencies are equal. This finding enhances the validity of the simpler rigid blade model for investigating the flap-lag stability characteristics of hingeless rotor blades in hover.

4. The effect of the number of elastic bending modes on the stability is generally small, especially where the rotor blade stiffness parameter is defined by the rotating natural frequency. Very accurate results for the lead-lag damping can be obtained with two modes for both the flap and lead-lag degrees of freedom.

5. For practical hingeless rotor blade configurations, the fundamental uncoupled flap and lead-lag rotating natural frequencies can be determined with acceptable accuracy by retaining the first two nonrotating bending modes for each degree of freedom.

6. Rotor blade pre-cone is generally stabilizing, although in some cases it is moderately destabilizing.

7. Rotary inertia effects are negligible for practical rotor blade configurations.

Ames Research Center
National Aeronautics and Space Administration
and
U. S. Army Air Mobility R & D Laboratory
Moffett Field, Calif., 94035, Nov. 8, 1972

REFERENCES

1. Hohenemser, Kurt H.; and Heaton, Paul W., Jr.: Aeroelastic Instability of Torsionally Rigid Helicopter Blades. J. Amer. Helicopter Soc., vol. 12, no. 2, April 1967, pp. 1-13.

2. Ormiston, R. A.; and Hodges, D. H.: Linear Flap-Lag Dynamics of Hingeless Helicopter Rotor Blades in Hover. J. Amer. Helicopter Soc., vol. 17, no. 2, April 1972, pp. 2-14.

3. Houbolt, John C.; and Brooks, George W.: Differential Equations of Motion for Combined Flapwise Bending, Chordwise Bending, and Torsion of Twisted Nonuniform Rotor Blades. NACA Rep. 1346, 1956.

4. Gessow, Alfred; and Myers, Garry S., Jr.: Aerodynamics of the Helicopter. Frederick Ungar Pub. Co., New York, 1967.

5. Chang, Tish-Chun; and Craig, Roy R., Jr.: On Normal Modes of Uniform Beams. Eng. Mech. Res. Lab. 1068, Univ. of Texas at Austin, Austin, Texas, 1969.

6. Felgar, Robert P., Jr.: Formulas for Integrals Containing Characteristic Functions of a Vibrating Beam. Univ. of Texas, Circular 14, Bur. Eng. Res., Austin, Texas, 1950.